ELSEVIER

Solar Energy Materials and Solar Cells 53 (1998) 67–82

Solar Energy Materials & Solar Cells

Design optimization of thermoelectric devices for solar power generation

S.A. Omer*, D.G. Infield

Department of Electronic and Electrical Engineering, CREST(Centre for Renewable Energy Systems Technology), Loughborough University, Loughborough, Leicestershire LE11 3TU, UK

Received 12 July 1997; received in revised form 2 December 1997; accepted 29 December 1997

Abstract

We present an improved theoretical model of a thermoelectric device which has been developed for geometrical optimization of the thermoelectric element legs and prediction of the performance of an optimum device in power generation mode. In contrast to the currently available methods, this model takes into account the effect of all the parameters contributing to the heat transfer process associated with the thermoelectric device.

The model is used for a comparative evaluation of four thermoelectric modules. One of these is commercially available and the others are assumed to have an optimum geometry but with different design parameters (thermal and electrical contact layer properties).

Results from the model are compared with experimental data of the commercial thermoelectric module in power generation mode with temperature gradient consistent with those achievable from a solar concentrator system. These show that it is important to have devices optimized specifically for generation, and to improve the contact layer of the thermoelements accordingly.

Keywords: Solar energy; Thermoelectric devices; Geometrical optimization of thermoelement; Thermoelectric device modelling; Contact resistance

1. Introduction

The direct conversion of the heat energy into electricity, or the reverse, by a thermoelectric device is related to electron transport phenomena, and the interrelated

* Corresponding author. E-mail: S.A.Omer@Lboro.ac.uk

0927-0248/98/$19.00
PII S0927-0248(98)00008-7

Seebeck, Petlier and Thomson effects. An exhaustive treatment of the basic theory is available in the literature [1–3].

In its simplest form, a thermoelectric circuit is formed of two dissimilar semiconductors, p- and n-type, connected electrically in series and thermally in parallel. Heat is supplied at one end whilst the other end is maintained at a lower temperature by a heat sink. As a result of the temperature difference, electrical current flows through an external load which completes the circuit.

Provided that the geometry of the thermoelement legs has been optimized, the performance of the thermoelectric material, and hence of the device, is characterized by a term known as the figure-of-merit $Z = S^2/Kr$ [1], where, S, r and K are the Seebeck coefficient, the electrical resistance and the thermal conductance, respectively, of the thermoelement. Therefore, a good thermoelectric material must posses a large Seebeck coefficient, high electrical conductivity and low thermal conductivity, a combination which is obtainable from semiconducting materials, or by adjustment of the stoichiometry and the optimum doping level of solid solution alloys [1].

A number of thermoelectric materials are available commercially [4]. One of these is the compound lead–telluride which has found use in power generation, and is useful in the temperature range 230–530°C [5]. Compounds based on bismuth–telluride are useful over the temperature range from room temperature to about 130°C [4]. For temperatures above 530°C, the best materials are the germanium–silicon alloys [6]. Both lead–telluride and germanium–silicon thermoelements are widely used for power generation, particularly for auxiliary power supply in space satellites, using isotope fuels [7], while bismuth–telluride thermoelements are mainly used for cooling purposes and low-scale power generation.

Semiconductor materials are relatively expensive, and therefore a design aim for a thermoelectric generator is to improve the power output per unit material. For solar energy applications this can be achieved by concentrating the solar radiation so as to create a high temperature gradient across the thermoelectric device [8], enabling minimal use of thermoelectric materials for a given power requirement. In addition, and more generally, the device should be optimized geometrically for maximum power output for a given thermoelectric material. Previously published optimization methods which are based on minimization of the term Kr, determine the ratio of lengths to areas of the p- and n-type element leg, but do not provide the actual dimensions. Moreover, important factors such as contact layer resistance and the contribution of the stray heat leakage to the cold junction through the space around thermoelement legs, are not always considered. Inevitably some heat leakage does take place between the hot plate and the cold plate via the space between the two plates. This heat transfer involves radiation, conduction and convection in the space between the plates if the device is not evacuated.

The contact layers (ceramic plates and electrical contact strips) result in thermal and electrical contact resistance at the two ends of the thermoelectric element. The thermal resistance as well as the stray heat leakage reduces the effective temperature difference across the element, and consequently the thermoelectric power, while the contact electrical resistance adds to the internal electrical resistance of the elements legs and thus affects the power output of the device.

Recently, Min and Rowe [9] have developed a procedure which considers the effect of contact layer resistance in the optimization of thermoelement leg, though, the effect of the stray heat leakage is not included. The stray heat term is determined principally by the thermoelement length, particularly when the space between the ceramic plates is not evacuated, and therefore should be considered in the optimization. The radiative heat exchange is not directly determined by the element length, however it is dependent on junction temperatures, which are in turn determined by the thermoelement length. In most of the published work the Thomson heat term is also neglected, on the assumption that it is relatively small. This is appropriate when the device is operated at a relatively low temperature gradient and for materials which do not show significant variation in the Seebeck effect with temperature. However, in the case of power generation which involves a high temperature gradient, the effect of the Thomson heat is appreciable and should be taken into consideration in order to avoid overestimation of the device performance.

Neglecting these heat terms both affects the optimum thermoelement length and overestimates the performance of the thermoelement. This can be seen from the relationship between efficiency and element length predicted using similar models and which indicate that the conversion efficiency continues to increase with element length.

In this paper, we present a theoretical thermoelectric model developed for geometrical optimization and the prediction of thermoelectric module performance. The model simulates real operational conditions by taking into account the effects of all the parameters discussed above.

For the sake of comparison, the optimization results are used for evaluation of several thermoelectric modules. One of the modules is a commercial thermoelectric cooling device, which can be used for power generation. The commercial device is evaluated using the current geometrical and contact layer properties as a base case. It is compared with a similar device, but with optimised element lengths. The other modules are assumed to have a similar geometrical structure, but with improved contact layer properties and optimum thermoelement lengths. All modules are based on bismuth–telluride thermoelectric alloys doped to give the best p-type and n-type materials (i.e., having figure of merit of about 3×10^{-3} per degree at room temperature [5]). The model predictions are compared with data from an experimental investigation of the commercial module under the same operating conditions.

2. An improved thermoelectric model

The section through the thermoelectric element, shown in Fig. 1 is used as a basis on which a set of formulae for the model are established. A module is formed from a number of thermoelectric couples, connected electrically in series and thermally in parallel, sandwiched between two thermally conducting and electrically insulating ceramic plates and sealed around the edges. The space between the two ceramic plates is filled with dry nitrogen gas.

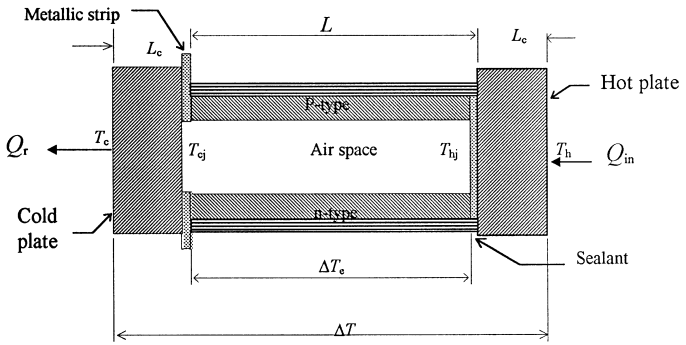

Fig. 1. Schematic diagram of thermoelectric element, showing the various components.

The properties of the thermoelectric materials are determined using the individual hot and cold junction temperatures. The material properties at these two temperatures are averaged for use in the model, as this procedure has been found to introduce minimal error [10]. The p- and the n-type thermoelectric pellets are assumed to be of uniform cross-section and equal in length.

The Seebeck coefficients of the p-type and n-type materials at the hot junction are $S_p(h)$ and $S_n(h)$, and at the cold junction $S_p(c)$ and $S_n(c)$, respectively. The electrical resistivities at the hot junction are $\rho_p(h)$ and $\rho_n(h)$, and at the cold junction $\rho_p(c)$ and $\rho_n(c)$. The thermal conductivity of the p- and the n-type elements at the hot junction is $k_p(h)$ and $k_n(h)$ respectively, and at the cold junction, $k_p(c)$ and $k_n(c)$.

Once a temperature gradient ΔT is established across the device, heat flows through thermoelement legs by direct conduction, and by radiation and conduction through the gas filled space between the two ceramic plates around the thermoelement legs, and through the sealant material.

A Seebeck emf will be induced across the terminals, and consequently if the circuit across the element is closed allowing a current I to flow, Peltier heat will be generated at each of the two junctions. The element absorbs heat at a rate equal to $S_h T_{hj} I$ at the hot junction and rejects heat at a rate equal to $S_c T_{cj} I$ at the cold junction. S_h and S_C are the average Seebeck coefficients at the hot and the cold junctions, respectively, of the p- and the n-pellets. At the same time, Thomson heat equivalent to $I\tau\Delta T_e$ will be generated in one of the element legs and absorbed in the other depending on the direction of the current flow, where, τ is the Thomson heat coefficient. Heat will also be generated along the element legs due to Joule heating within each leg.

The heat entering the hot junction, is the sum of the heat input from the hot source Q_{in}, and the proportions of the Joule and the Thomson heats transported to the hot junction. The heat leaving the hot junction is equal to the sum of the heat conducted to the cold junction via thermoelement legs, the Peltier heat absorbed by the charge carriers, conduction via the sealant and the gas-filled space and the radiative exchange between the hot plate and the cold plates.The energy balance gives

$$Q_{in} = Q_C(h) + Q_P(h) + Q_{sp} + Q_{seal} - f_t Q_t - f_j Q_j, \tag{1}$$

where $Q_C(h)$, $Q_P(h)$, Q_t, Q_j, Q_{sp} and Q_{seal} are the heat flow by conduction through thermoelement legs, the Peltier heat, the Thomson heat, the Joule heat, the heat leakage via the space and the heat leakage via the sealant material to the cold junction. $f_j = f_t = 0.5$ [11,12] are the fractions of the Joule and the Thomson heats fed back to the hot junction.

To determine these heat terms and the electrical output power, we need to estimate the effective temperature of the thermoelement junctions. As mentioned earlier, the contact layers result in thermal and electrical contact resistance's at the two ends of the thermoelectric element. The thermal resistance causes the effective temperature difference across the elements to be ΔT_e Te rather than ΔT, as shown in Fig. 1. This effective temperature difference is also dependent on the rate at which heat flows to the cold junction, including the thermoelectric effects and the stray heat leakage. The contact electrical resistance adds to the electrical resistance of the elements legs, and thus limits the useful electrical power output.

Taking into account the contact electrical resistance of the junction layers, the total internal resistance of a thermoelectric couple can be expressed as follows [1]:

$$r = 2r_c + 2\rho\frac{L}{A} = \frac{2\rho}{A}\left(\frac{r_c A}{\rho} + L\right) = \frac{2\rho}{A}\left(\frac{\rho_c}{\rho} + L\right) = 2\rho(\rho_{oc} + L)/A, \tag{2}$$

where $\rho_{oc} = \rho_c/\rho$, and the quantity $\rho_c = r_c A$ characterizes the quality of the junction; $r_c \propto A^{-1}$ is the contact resistance at each junction (hot or cold), $\rho = (\rho_p + \rho_n)/2$ is the bulk electrical resistivity of the thermoelectric materials at a given temperature, A is the cross-sectional area and L is the length of the thermoelement.

Effects due to the contact thermal resistance and the heat leakage from the hot plate to the cold plate can now be considered. A procedure is employed which estimates the temperature distribution across the thermoelectric device, allowing the effective temperature difference ΔT_e across the hot and the cold junctions to be evaluated. The analysis is undertaken by considering T_h and T_c to be the temperatures of the outer surface of the hot and the cold ceramic plates, respectively, and T_{hj} and T_{cj} the corresponding inner surfaces temperatures, respectively, at the metallic bridge contact points. It can be assumed that the gas-filled space between the two ceramic plates is at a mean temperature $T_m = 0.5(T_h + T_c)$, at which its thermal properties are evaluated.

For simplicity, one-dimensional heat flow is assumed. This is reasonable, since the ceramic plates are usually thin and therefore heat flow along the plates due to local temperature gradients can be neglected compared to heat flux across the plates. Heat losses from the side edges can also be neglected. Considering an open circuit condition for simplicity, an equivalent thermal network for the thermoelectric element is shown in Fig. 2.

The total heat flux Q_{FL} from the heat source to the heat sink through the thermoelectric module is given by

$$Q_{FL} = (\sum R_{th})^{-1}(T_h - T_c), \tag{3}$$

where $\sum R_{th}$, is the total thermal resistance to the heat flow through the thermoelectric module.

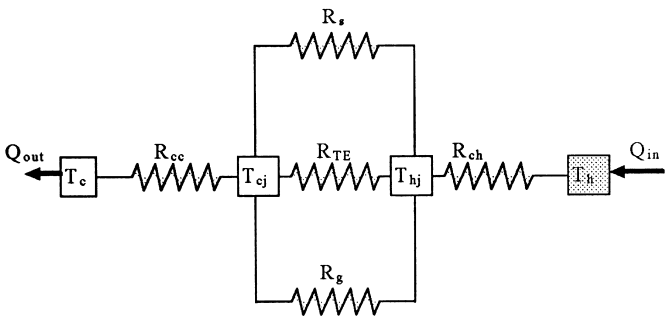

Fig. 2. Equivalent thermal network for heat transfer across a thermoelectric module.

Under steady-state and open-circuit conditions, the heat flow rate through the hot and cold ceramic plates is identical and equal to the heat flux through the module. Therefore, the effective temperature difference between the hot and the cold contact points can be estimated as follows:

$$T_{hj} = T_h - R_c \Delta T / \sum R_{th}, \tag{4}$$

$$T_{cj} = T_c + R_c \Delta T / \sum R_{th}, \tag{5}$$

where R_c is the thermal resistance to the heat flow through the ceramic plates.The effective temperature difference, $\Delta T_e = T_{hj} - T_{cj}$, is given by

$$\Delta T_e = \left(1 + 2\frac{L_C}{L}\frac{U}{k_{oc}A_{oc}}\right)^{-1} \Delta T, \tag{6}$$

where L_c is the thickness of the ceramic plate, k_{oc} is the ratio of the thermal conductivity of the ceramic plate to that of the thermoelement, A_{oc} is the corresponding ratio of the cross-sectional areas, U is a factor that accounts for the thermal resistance to the stray heat leakage from the hot junction to the cold junction, and is given by [13]

$$U = 1 + k_{os}A_{os} + k_{og}A_{og} + \frac{\varepsilon\sigma A_{og}}{2-\varepsilon}\frac{L}{k}(T_{hj}^2 + T_{cj}^2)(T_{hj} + T_{cj}), \tag{7}$$

where k_{os} and k_{og} are the ratios of the thermal conductivity's of the sealant and the gas-filled space, respectively, to that of the thermoelement, A_{os} and A_{og} are the corresponding ratios of the cross-sectional areas, $k = k_p + k_n$, is the thermal conductivity of the thermoelement couple. $\sigma = 5.67 \times 10^{-8}$ W m^{-2}K^{-4} is the Stefan–Boltzmann constant and ε is the emmisivity of the ceramic plate surface. For simplicity, the hot and the cold ceramic plates surfaces are assumed to have the same emmisivity, and are approximated as infinitely long parallel plates.

It can be shown [13] that Eq. (7), together with Eqs. (4)–(6) give the following cubic equation for U:

$$C_1^2U^3 + (2C_1 - C_2 - C_3C_1^2)U^2 + (1 - 2C_1C_3)U - C_3 = 0, \tag{8}$$

where

$$C_1 = 2\frac{1}{L}\frac{L_c}{A_{oc}k_{oc}}, \quad C_2 = \frac{4\varepsilon\sigma A_{og}}{2-\varepsilon}\frac{1}{Lk}\left(\frac{L_c}{A_{oc}k_{oc}}\right)^2(\Delta T)^2\bar{T}$$

and

$$C_3 = 1 + k_{os}A_{os} + k_{og}A_{og} + \frac{2\varepsilon\sigma A_{og}}{2-\varepsilon}\frac{L}{k}(T_h^2 + T_c^2)\bar{T}.$$

Under matched load conditions and at given hot and cold junctions temperatures, the electrical current I_M per unit area through the circuit, the terminal voltage V_M per couple and the power output P_M per couple as a function of thermoelement geometry, for temperature difference ΔT, can be calculated by introducing the average value of the Seebeck coefficient $\bar{S}$ as follows:

$$I_M = \frac{\bar{S}}{4\rho}(\rho_{oc} + L)^{-1}\left(1 + 2\frac{L_c}{L}\frac{U}{k_{oc}A_{oc}}\right)^{-1}\Delta T, \tag{9}$$

$$V_M = \frac{\bar{S}}{2}\left(1 + 2\frac{L_c}{L}\frac{U}{k_{oc}A_{oc}}\right)^{-1}\Delta T, \tag{10}$$

$$P_M = \frac{\bar{S}^2}{8\rho}(\rho_{oc} + L)^{-1}\left(1 + 2\frac{L_c}{L}\frac{U}{k_{oc}A_{oc}}\right)^{-2}(\Delta T)^2, \tag{11}$$

where U is calculated by solving the cubic Eq. (8).The optimum element length can be obtained by plotting power against element length for given operational conditions.

The energy input to the thermoelectric device can be obtained by substituting for $Q_C(h)$, $Q_P(h)$, Q_t, Q_j, Q_{sp} and Q_{seal} in Eq. (1). The thermoelectric heat to electrical power conversion efficiency as a function of the gross temperature difference ΔT across the device, is obtained from Eqs. (1) and (11):

$$\eta = \frac{P_M}{Q_{in}} = \frac{\Delta T}{C_4}\left(\begin{array}{l}\dfrac{2S_h}{\bar{S}}\left(T_h - \dfrac{\Delta T}{C_6}\right) - \dfrac{\bar{T}\Delta\bar{S}}{\bar{S}} + \dfrac{8\rho k}{\bar{S}^2}C_5C_7 \\ \quad - \dfrac{\Delta T}{2C_4} + C_7C_8\dfrac{\rho\bar{T}}{\bar{S}^2}\left(T_h^2 + T_c^2 + \dfrac{2}{C_6^2}\Delta T^2\right)\end{array}\right)^{-1} \tag{12}$$

where

$$C_4 = \left(1 + 2\frac{L_c}{L}\frac{U}{k_{oc}A_{oc}}\right), \quad C_5 = 1 + k_{os}A_{os} + k_{og}A_{og}, \quad C_6 = C_4\frac{L}{L_c}\frac{A_{oc}k_{oc}}{U},$$

$$C_7 = (\rho_o + L)L^{-1}, \quad C_8 = 32\varepsilon\sigma A_{og}(2-\varepsilon)^{-1}.$$

Eq. (12) is valid when the device is operated at maximum power output. The effect of the contact resistance at the junctions, the Thomson heat and the stray heat leakage has been properly taken into account.

3. Experimental investigation

The thermoelectric device DT1089 obtained from Marlow Industries Inc. USA, was selected for test purposes. The hot ceramic plate was painted black to improve the absorptance to the incident radiation. A variable load resistance was connected across the terminals of the device to allow measurement of the current–voltage characteristics of the device.

The heat source was provided by concentrating light from a 175 W infrared heat lamp using a conical concentrator with a concentration factor of 6, designed to provide a uniform radiation on the surface of the device. With this arrangement a radiant power of 2 W/cm^2 was obtained on the surface of the ceramic plate.

The cold-junction temperature was maintained by circulating cold water through a heat exchanger attached to the cold plate of the thermoelectric device. The test was carried out for various hot and cold junctions temperatures and varying load resistance.

4. Results and discussion

4.1. Theoretical results

Calculations were based upon published temperature-dependent properties of bismuth telluride materials, and contact layer properties available in the literature [5,9]. The materials used for the ceramic plates are commonly aluminum oxide (alumina) or beryllium oxide due to their good thermal conductivity and electrical insulation properties [14]. They are categorized as aluminum oxide ceramics (AC), beryllium oxide ceramics (BC) or a combination of aluminum and beryllium oxide ceramics (AB). The metallic conductors are made of copper strips affixed to the ceramics by a variety of methods, the most common of which is to print and fire a circuit pattern using molymanganese or copper. The copper conductors are then soldered to this circuit pattern [14]. The elements are soldered to the electrical conductors using bismuth tin solder (melting point = 138°C) as is the case of the commercial Peltier cooling devices, or by using tin lead solder (melting point = 183°C). The junction quality is determined by the quality of the contact surface and soldering.

The commercial device considered for comparative evaluation, was principally developed for Peltier cooling as mentioned earlier. However, it has been suggested that it can be used for power generation [15]. The device is a single-stage thermoelectric module comprising a matrix of 127 thermoelectric couples (p- and n-type) sandwiched between two aluminum oxide plates and connected in series using eutectic

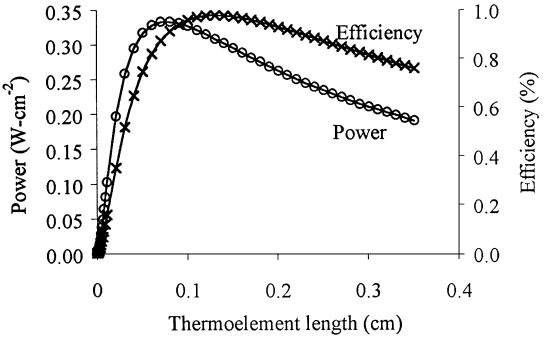

Fig. 3. Variation of the power output and conversion efficiency with thermoelement length.

BiSn solder which melts at approximately 138°C, and therefore, the maximum operating temperature of the device is limited to this. The space between the two ceramic plates is filled with dry nitrogen gas and sealed using an RTV sealant to improve its reliability in condensing environments. Materials used to prepare this device are claimed to have the highest thermoelectric figure-of-merit [15].

Fig. 3 illustrates the variation of the power output per unit area and the conversion efficiency with thermoelement length for $k_{oc} = 2.5$ and $\rho_{oc} = 0.1$, and hot and cold junctions temperatures of 127°C and 57°C. It can be observed that, the maximum efficiency is obtained for an element length longer than that which gives the maximum power. Using the element length which gives maximum power will result in a drop in the conversion efficiency of a few percent. For example, at a temperature difference 70°C, the optimum length for maximum power is 0.075 cm, rather than 0.13 cm for maximum efficiency. Optimising length for maximum power will result in a 21% increase in the power output, accompanied by 8% drop in the efficiency compared to a design based on maximum efficiency. In conclusion optimization of length for maximum power will improve the power output per unit material and hence the cost effectiveness of the device, despite some reduction in efficiency. For solar applications the latter is cost effectively compensated for by increasing the degree of concentration [8].

Figs. 4 and 5 show the variation of the maximum power output and the corresponding optimum thermoelement length with contact layer resistance. It can be observed that, the thermoelement length which gives the maximum power varies substantially with both electrical and thermal contact resistance. This indicates the importance of marginal improvements in contact design.

A thermoelectric device with a high conductivity (both electrical and thermal) for the contact layers can be combined with a short element and deliver high power output. Poor contact layers result in a device that requires a long thermoelement and yields low power per unit area. This is because low thermal conductivity results in a high temperature gradient at the contact points, and a consequent drop in the effective temperature difference between the two junctions. On the other hand, contact

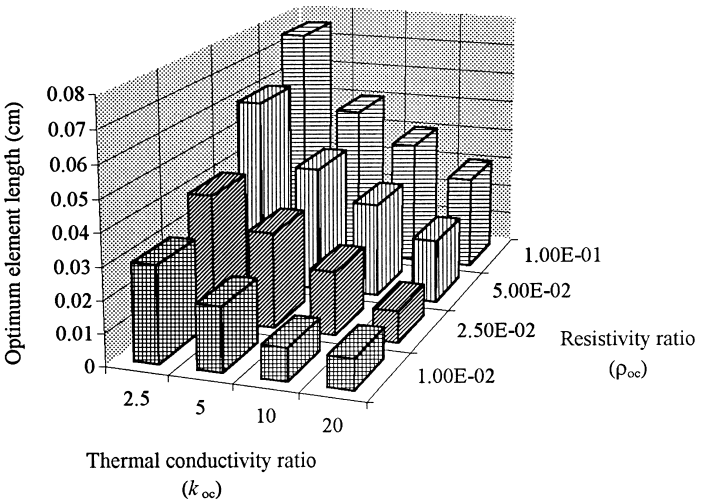

Fig. 4. Variation of the optimum thermoelement length with the contact layer resistance.

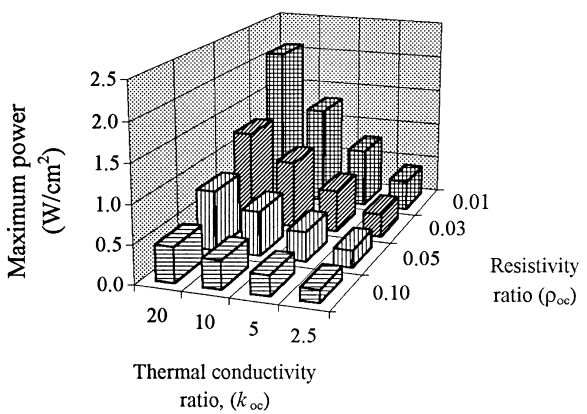

Fig. 5. Variation of maximum power with contact layer resistance.

layers with high electrical resistivity mean that the internal resistance of the device will be dominated by the contact resistance, and the performance of the device will be poor.

Fig. 6 compares the results of the current model (denoted by subscript cm) with a representation which does not take into account the effect of Thomson heat and the stray heat leakage (denoted by subscript pm), for $k_{oc} = 2.5$, $\rho_{oc} = 0.1$, and hot and cold junctions temperatures of 127°C and 57°C, respectively. It can be seen clearly that neglecting these two heat terms results in a long thermoelement and an overestimate

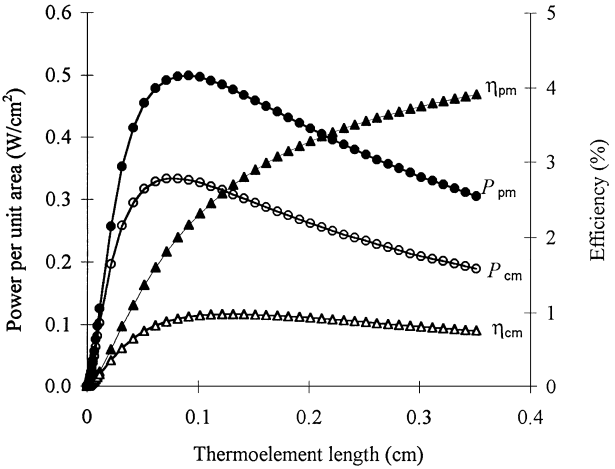

Fig. 6. Comparison between model results and previously published results (P_{pm} and η_{pm} are the power and efficiency of the published models and P_{cm} and η_{cm} are the power and efficiency of the current model).

of device performance. The efficiency curve calculated from the previously published models shows a continuous increase in efficiency with thermoelement length. This is because, the stray heat is determined by the effective temperature difference which is dependent on the thermoelement length, and both determine the rate of heat flux through the device. Neglecting the stray heat leakage will result in an underestimate of the heat flux through the device and consequent underestimation of the energy input to the device. These results show that neglecting these heat terms results in an overestimate of the optimum element length, power output and conversion efficiency by about 18%, 33% and 57%, respectively, compared to the predictions of the model presented here.

Results from the optimization have been used in a comparative evaluation of four different thermoelectric modules. The first module is the commercial module with its current geometrical and contact layer properties. The second module is similar to the first one, but with the optimum thermoelement length as calculated using the current model. The other two modules are assumed to have optimum lengths and also improved contact layer properties.

The geometrical and the other technical parameters of the four modules considered are presented in Table 1.

Power delivered to a matched load, as a function of junction temperature, for the four modules is given in Fig. 7.

4.2. Experimental results

Fig. 8 shows the I–V characteristics and power curve for hot and cold junction temperatures of 127°C and 27°C. For a 100°C temperature difference, the open-circuit

Table 1
Details of the four modules considered for comparative evaluation

MODULE	Length (mm)	k_{oc}	r_{oc}	Remarks
Module-1	1.4	2.5	0.1	Commercial module
Module-2	0.75	2.5	0.1	Module-1, L(optimum)
Module-3	0.4	10	0.1	k_c improved, L(optimum)
Module-4	0.3	2.5	0.01	r_c improved, L(optimum)

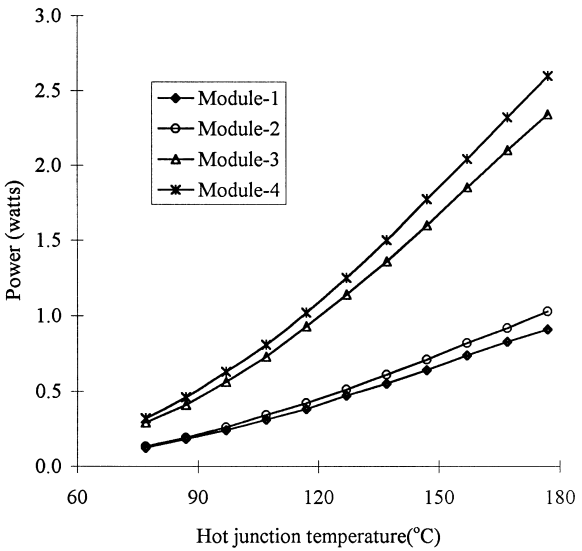

Fig. 7. Variation of power output into a matched load with junction temperature, for the four modules.

voltage and the short-circuit current are 2 V and 0.6 A, respectively. As can be seen, the power curve is parabolic, with maximum power at half the open-circuit voltage. In contrast to photovoltaic cells, the maximum power point of the thermoelectric module is always obtained at half the open-circuit voltage due to the linear I–V characteristics. This emphasises the importance of the internal resistance in determining the performance of a thermoelectric device.

Fig. 9 shows the variation of the maximum power delivered into a matched load, together with the voltage, current and efficiency at the maximum power point, as a function of hot junction temperature. Though the output voltage continues to increase with temperature difference, the current and consequently the maximum power and the conversion efficiency reach a maximum value between 70°C and 90°C. When the device is operated as a cooler, this limiting temperature difference is known

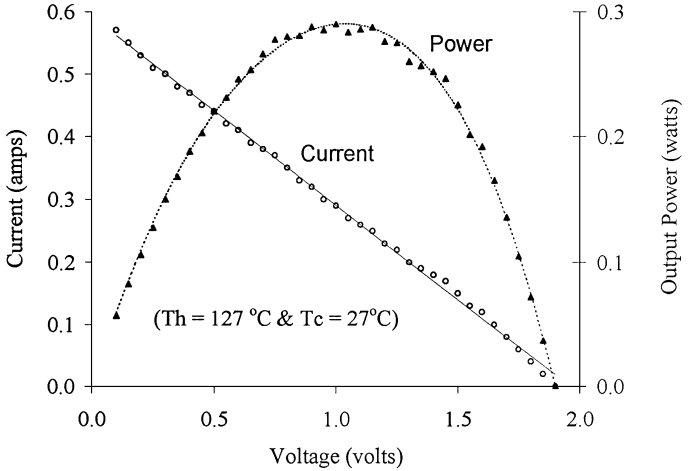

Fig. 8. current–voltage characteristics and power output for hot- and cold-junction temperatures of 127°C and 27°C, respectively.

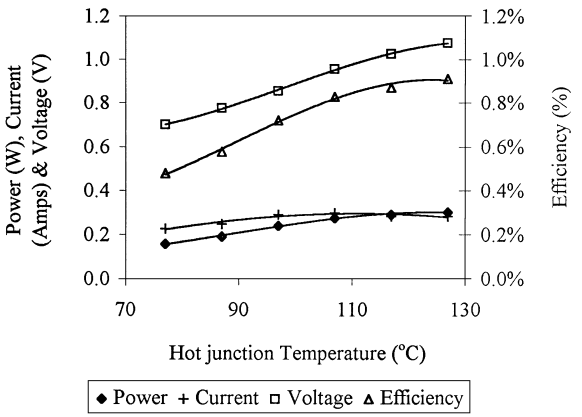

Fig. 9. Variation of thermoelectric device performance with hot-junction temperature for a cold-junction temperature 27°C.

as the maximum no-load temperature difference. One of the factors that determines this maximum is the thermoelectric material itself, and its electron transport properties. The maximum power output obtained at a temperature difference of 100°C is about 0.3 W, with an overall solar to electricity conversion efficiency of about 0.9%.

4.3. Validation of the theoretical model

Data obtained from the experiment has been used to validate the thermoelectric model presented. Fig. 10 compares the predicted and measured power delivered into

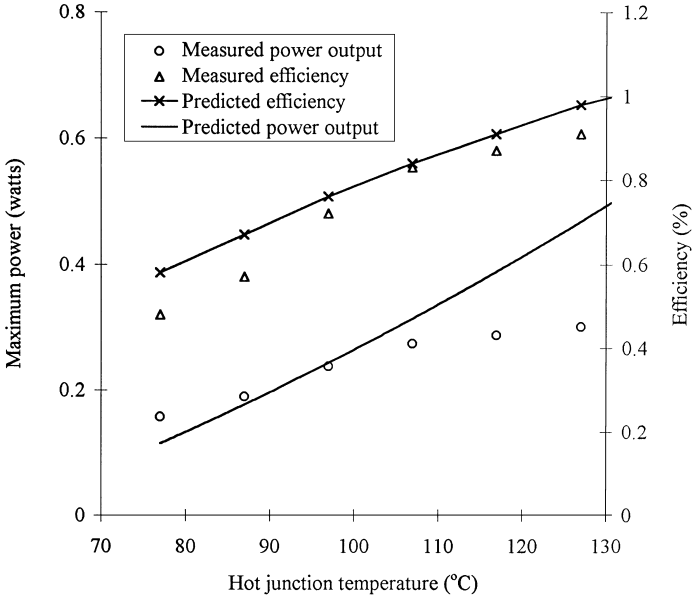

Fig. 10. Comparison between predicted and measured results for the commercial device.

a matched load, and the corresponding conversion efficiencies, as a function of the hot-junction temperature, for a cold-junction temperature of 27°C.

It can be observed that, whilst the predicted power performance continues to increase with the junction temperature up to the maximum temperature considered in this evaluation, the measured performance reaches a maximum value at a temperature difference of about 70°C. This can be attributed to two main factors. First, that the power is proportional to the product of the square of temperature difference and the square of the Seebeck coefficient, so that as the temperature difference increases, the ΔT^2 term primarily determines the power output. The decrease in the Seebeck coefficient which has been incorporated into the model, based on published data, is too small to compensate for this increase. However, at low temperatures, there is good agreement between the predicted performance and measurement. The second factor relates to assumptions made in the model regarding the radiation properties of the surfaces and the contact layer properties, which are taken to be constant over operating temperature range.

In context of these comments, the level of agreement between the model and the measured data is encouraging, and gives confidence in the accuracy of the model, at least under the operational conditions investigated.

5. Conclusions

An improved thermoelectric model has been developed which allows geometrical optimization of the thermoelement and prediction of the performance of an optimum device in power generation mode. The model considers the effect of all the parameters that contribute to the heat transfer process associated with thermoelectric devices in power generation mode, some of which have been ignored in previous models. The optimization of the element length performed here is based on maximum power output from the device, and not efficiency.

The model is used to optimize the thermoelement dimensions for various contact layer properties, and to predict the theoretical performance of a commercial Peltier cooling device in power generation mode. This commercial device is compared with three other module designs based on optimum thermoelement length and with improved contact layer properties. The comparison indicated that the performance of the commercial Peltier device is inferior to those based on optimum element length, particularly those with improved contact layers. This emphasizes the importance of optimizing thermoelectric generators on the basis of maximum power, rather than efficiency, particularly when designs are being considered for applications where the cost of the energy input is low, as in the case of solar energy converters. The results also highlight the importance of using devices with improved contact layer properties.

A comparison of the results with those from previously published models showed that the current model represents the energy transfer mechanisms associated with thermoelectric devices in a manner that gives improved agreement with experimental results.

References

[1] A.F. Ioffe, Semiconductor Thermoelements and Thermoelectric Cooling, Infosearch, London, 1957.
[2] I.B. Cadoff, E. Miller, Thermoelectric Materials and Devices, Material Technology Series, Chapman and Hall, London, 1960.
[3] D.D. Pollock, Thermoelectricity, Theory Thermometry Tool, ASTM, Wiley, New York, 1985.
[4] H.J. Goldsmid, Bismuth Telluride, in: C.A. Hogarth (Ed.), Materials used in Semiconductor Devices, Interscience, New York, 1965.
[5] S.I. Freedman, Thermoelectric devices, in: G.W. Sutton (Ed.), Direct Energy Conversion International University Electronic Series, McGraw-Hill, New York, 1966.
[6] J.P. Dismukes, F.D. Rossi, GeSi alloys for thermoelectric power generation – a review, A.I.CH.E Int. Chem. Eng. Symp. Series, 5, 1965.
[7] G.L. Bennet, Application of thermoelectric in space, in: D.M. Rowe (Ed.), CRC Handbook of Thermoelectric, CRC Press, Boca Raton, 1995.
[8] S.A. Omer, D.G. Infield, Design of a two-stage solar concentrator for thermoelectric power generation, Solar Energy, 1997, Submitted for publication.
[9] Min Gao, D.M. Rowe, Power Source 38 (1992).
[10] P.H. Egli, Thermoelectricity, Wiley, 1960.
[11] A.D. Burstein, Soviet Phys. Tech. Phy. 2 (7) (1958) 1397–1406.
[12] R.W. Cohen, J. Phy. 34 (6) (1963).

[13] S.A. Omer, Solar thermoelectric system for small scale power generation, Ph.D. thesis, Loughborough University, UK, 1997.
[14] R.B. Burke, Thermoelectric coolers as power generators, 18th Intersociety Energy Conversion Engineering Conference, August 1983, pp. 21–26.
[15] R.E. Marlow, E. Burke, Module design and fabrication, in: D.M. Rowe (Ed.), CRC Handbook of Thermoelectric, CRC Press, Boca Raton, 1995.